Spectroscopy and coherent manipulation of single and coupled flux qubits*

Wu Yu-Lin(吴玉林), Deng Hui(邓 辉), Huang Ke-Qiang(黄克强), Tian Ye(田 野), Yu Hai-Feng(于海峰), Xue Guang-Ming(薛光明), Jin Yi-Rong(金贻荣), Li Jie(李 洁), Zhao Shi-Ping(赵士平), and Zheng Dong-Ning(郑东宁)†

Beijing National Laboratory for Condensed Matter Physics, Institute of Physics, Chinese Academy of Sciences, Beijing 100190, *China*

(Received 26 March 2013; revised manuscript received 19 April 2013)

Measurements of three-junction flux qubits, both single flux qubits and coupled flux qubits, using a coupled direct current superconducting quantum interference device (dc-SQUID) for readout are reported. The measurement procedure is described in detail. We performed spectroscopy measurements and coherent manipulations of the qubit states on a single flux qubit, demonstrating quantum energy levels and Rabi oscillations, with Rabi oscillation decay time $T_{\rm Rabi} = 78$ ns and energy relaxation time $T_1 = 315$ ns. We found that the value of $T_{\rm Rabi}$ depends strongly on the mutual inductance between the qubit and the magnetic coil. We also performed spectroscopy measurements on inductively coupled flux qubits.

Keywords: quantum computing, flux qubit, Rabi oscillation, dc-SQUID

PACS: 03.67.Lx, 85.25.Cp, 85.25.Dq, 85.25.Hv **DOI:** 10.1088/1674-1056/22/9/090312

1. Introduction

Based on the basic properties of quantum mechanics such as entanglement and state superposition, quantum information processing[1], once realized, has long been recognized as having a much stronger computational power in comparison with classical information processing. The basic unit of quantum information processing is a quantum two-level system, called a qubit. Though the qubit has been successfully implemented in many different physical systems such as nuclear magnetic resonance (NMR), trapped ions, cavity-quantum-electro-dynamics (CQED), and solid state systems,[2–9] there are still great challenges toward realizing practical quantum information circuits. Among these challenges, two are especially important: one is obtaining a long coherence time, and the other is a controllable coupling between qubits or scalability. Qubits based on NMR and trapped ions have long coherence time, but scalability in these qubit systems is difficult. In comparison, scalability to a large structure is straightforward for qubits based on solid state systems due to their well established micro fabrication techniques. One drawback of the solid state qubits is their relatively short coherence time. For this reason, superconducting qubits,[5,10] i.e., qubits based on Josephson junctions, are especially attractive, as the superconducting state is separated from the normal state by an energy gap and is a dissipationless state, a relatively longer coherence time can be achieved in superconducting qubits in comparison to other types of solid state qubits.

Superconducting qubits utilize the nonlinear property of Josephson junctions[11] to form a quantum two-level system suitable for quantum information manipulation and storage. As the superconducting state is an intrinsic coherent state, superconducting qubits behave like natural atoms in many aspects despite their huge dimensions, which could be as large as several hundred micrometers. For this reason, besides serving as promising candidates for realizing quantum information processing, superconducting qubits can also be taken as artificial atoms, giving rise to a rich field for demonstrating and testing fundamental quantum mechanical phenomena on a macroscopic scale.[12] Such artificial atoms have great advantages over the natural atoms because of their design flexibility, and they can easily be tuned by external parameters such as a magnetic flux. Different types of superconducting qubits, such as charge qubits,[13] quantroniums,[14] flux qubits,[15–20] and phase qubits,[21] have been realized in the last two decades. Intensive research works, both theoretical and experimental, have been done in the field of superconducting qubits, and exciting results like the coherent manipulation of the qubit quantum states have also been demonstrated. Nevertheless, realizing practical quantum information circuits still remains a challenging task. A lot of critical problems have yet to be solved. In this paper, we present our work on the measurements of flux qubits, both single flux qubits and coupled flux qubits.

The type of flux qubit we study is the three-junction flux qubit, or the persistent-current qubit.[15] It is a low inductance superconducting loop interrupted by three sub micron sized Josephson junctions (Fig. 1(a)); two of these junctions have equal junction areas, and the other one has a junction area that is α times smaller ($0.5 < \alpha < 1$). The value of α, together

*Project supported by the National Basic Research Program of China (Grant Nos. 2011CBA00106 and 2009CB929102), the National Natural Science Foundation of China (Grant Nos. 11104333, 10974243, 11104340, and 11161130519), and the Knowledge Innovation Program of the Chinese Academy of Sciences.

†Corresponding author. E-mail: dzheng@aphy.iphy.ac.cn

© 2013 Chinese Physical Society and IOP Publishing Ltd

with the Josephson energy $E_J = hI_c/4\pi e$ and charging energy $E_c = e^2/2C$, characterize the flux qubit, where h is Planck's constant, I_c and C are the critical current and the junction capacitance of the big junctions, respectively. The ratio of E_J/E_c is typically $10 < E_J/E_c < 100$. With appropriate parameters, if the flux threading the qubit loop Φ_e is around $(n+1/2)\Phi_0$, where n is an integer, $\Phi_0 = h/2e$ is the flux quantum, the flux qubit has a double-well potential with two minima separated by an energy barrier (Fig. 1(b)). The classical states in these two minima correspond to opposite circulating currents $\pm I_p$ in the loop, and tunneling between the two minima leads to suppositions of these two states. On the basis of these two circulating current states, $|+\rangle$ and $|-\rangle$, the Hamiltonian of the flux qubit can be written as[15]

$$H_{qb} = -\frac{1}{2}(\varepsilon\sigma_z + \Delta\sigma_x), \tag{1}$$

where σ_z and σ_x are the Pauli matrices, $\varepsilon = 2I_p(\Phi_e - (n+1/2)\Phi_0)$, Δ is the tunnel coupling between the two circulating current states. The energy difference between the lowest two qubit eigenstates $|0\rangle$ and $|1\rangle$ is $E_{01} = \sqrt{\varepsilon^2 + \Delta^2}$. The circulating currents of these two qubit states are $\langle I_{pi}\rangle = -\partial E_i/\partial\Phi_e$ (Fig. 1(c)). They have opposite signs and vanish at the symmetric point $(n+1/2)\Phi_0$.

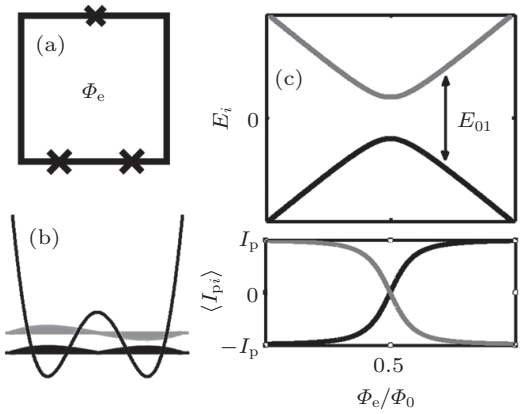


Fig. 1. (a) Schematic diagram of the three-junction flux qubit. Crosses are Josephson junctions. (b) Double-well potential of flux qubit at the symmetric point $\Phi_e = (n+1/2)\Phi_0$ and schematic diagram of the two lowest energy eigenstates. The vertical axis is energy; the horizontal axis is the phase coordinate. (c) Energy levels and circulating currents in the qubit loop of the two lowest energy eigenstates as a function of flux threading the qubit loop Φ_e.

A readout of the qubit state can be performed by inductively coupling a direct-current superconducting quantum interference device (dc-SQUID) to the qubit loop to measure the flux generated in the SQUID loop by the circulating current of the qubit. For the ground and excited states, the fluxes are in two opposite directions. This leads to the total flux (that is, the external bias flux plus the flux generated by the qubit) detected by the dc-SQUID differing slightly for the two qubit states. Consequently, the switching current of the dc-SQUID, which is under-damped, will be slightly different too. Close to the symmetric point, the circulating current in the qubit loop vanishes or is too small to be directly detected by the readout SQUID, the qubit has to be adiabatically shifted away from the symmetric point by using a rectangular shift flux bias pulse during the readout process. To reduce back actions of the readout SQUID to the qubit, the readout SQUID is only weakly coupled to the qubit.

2. Sample and measurement setup

Our samples are fabricated on thermally oxidized silicon substrates (the oxidation layer is 500 nm in thickness) as described previously.[22] In brief, big structures such as on-chip resistors, bonding pads, and the bottom planes of shunting capacitors are fabricated using photolithography and thin film deposition. Two separate steps are involved. The first step is to fabricate the bottom planes of shunting capacitors, which are thin films of aluminum heavily oxidized after deposition to form an insulating layer on the surface. The second step is the fabrication of bonding pads and on-chip bias resistors, which are thin films of gold. This gold layer also serves as a quasiparticle trap. Small structures such as qubits, readout SQUIDs, and the top planes of shunting capacitors are fabricated using electron beam lithography and aluminum thin film deposition. Key elements of the qubits and the readout SQUIDs are Josephson junctions; they are formed by using the well known Dolan bridge double-angle shadow evaporation technique.[23] The qubit loop is 20 μm×20 μm, and the SQUID loop is 24 μm×24 μm. The mutual inductance M_{sq} between them is 28 pH. The junction sizes of the large junctions of the qubit and the junctions of the SQUID are 0.074 μm^2. The ratio α is 0.76. The critical current density of the junctions is about 0.34 kA/cm^2, the critical current of the SQUID junctions is about 250 nA each. The junction capacitance is about 110 fF/μm^2. The shunting capacitor of the readout SQUID (C_{sh}) is about 10 pF. This capacitor is made on-chip, together with an on-chip bias resistor, to form a resistor–capacitor (RC) filter.

After fabrication, the samples are cut into 6 mm×6 mm chips. The chip to be measured is mounted into a copper sample holder to shield it from radio-frequency (rf) radiations. The sample holder is thermally attached to the mixing chamber of a dilution refrigerator with a base temperature of about 30 mK.[24] The dilution refrigerator is shielded with three μ-metal layers at room temperature to provide a stable magnetic environment for the sample.

Figure 2 shows the schematic diagram of the measurement setup. All control and readout pulses are generated by a computer controlled 4-channel arbitrary waveform generator (AWG). The readout and microwave pulses are sent to the

sample by wide bandwidth coaxial cables, attenuated at different temperature stages of the dilution refrigerator. Down at the base temperature the readout pulses go through a copper powder filter (CPF) for filtering the high frequency noises and then are converted to current bias pulses for the readout SQUID by the bias resistor. In our measurement setup, the bias resistor consists of an on-chip resistor of 250 Ω and a 5 kΩ resistor mounted outside the sample holder in series. The microwave pulses are coupled to the qubit through the mutual inductance between the on-chip microwave antenna and the qubit loop. Switching voltage signals go through a CPF and several RC filters (RCF) before reaching the room temperature amplifier. The magnetic flux bias for the qubit and the SQUID is provided by a niobium superconducting coil close to the sample. The bias line and voltage line of the readout SQUID go through several stages of filtering to obtain a sufficient isolation of the readout SQUID from the external environment.

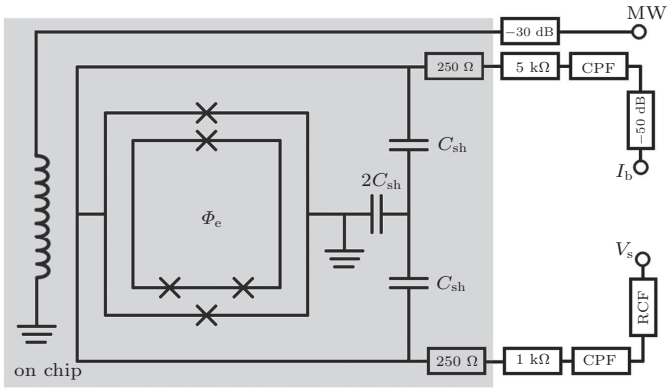


Fig. 2. Schematic diagram of the measurement setup. Shaded area is on chip.

3. Measurement

To detect the qubit state, a short readout pulse, several nanoseconds typically, is sent through the bias line to the readout SQUID, which switches to the voltage state with some probability. The switching voltage signal V_s of the readout SQUID is sent out to a low noise differential amplifier at room temperature and the amplified signal is then sent to a threshold detector to determine the occurrence of switching. Due to heavy filtering, the bandwidth of the voltage line is usually no more than a few MHz; for this reason the short readout pulse has a trailing hold plateau with an amplitude just above the retrapping current of the readout SQUID to maintain it in the voltage state for a sufficiently long time for the amplifier to pick up the voltage signal (Fig. 3). The switching probability is obtained by averaging over N measurements. To choose the proper N, we measure the switching probability versus N (Fig. 4(a)). The value of P should converge to a probability value after N exceeds some value, typically several thousands, and this is the proper value for N. If P is not convergent (Fig. 4(b)), then the measurement system is unstable over time, and unknown noise or perturbation sources have to be tracked out before any further measurement is possible. In our measurements, N is typically 8000. After each measurement, the qubit is relaxed to the ground state $|0\rangle$ by waiting a sufficiently long time before the next qubit state manipulation and readout sequence. We perform our measurement at a repetition rate of 16 kHz.

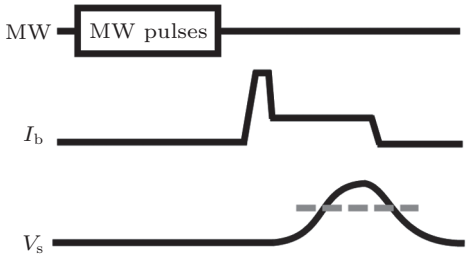


Fig. 3. Schematic representation of the flux qubit microwave control pulses, SQUID readout pulse I_b, and switching voltage signal V_s. The switching voltage signal V_s is amplified by a low noise amplifier at room temperature, and a threshold detector (dashed line) determines the occurrence of the switching.

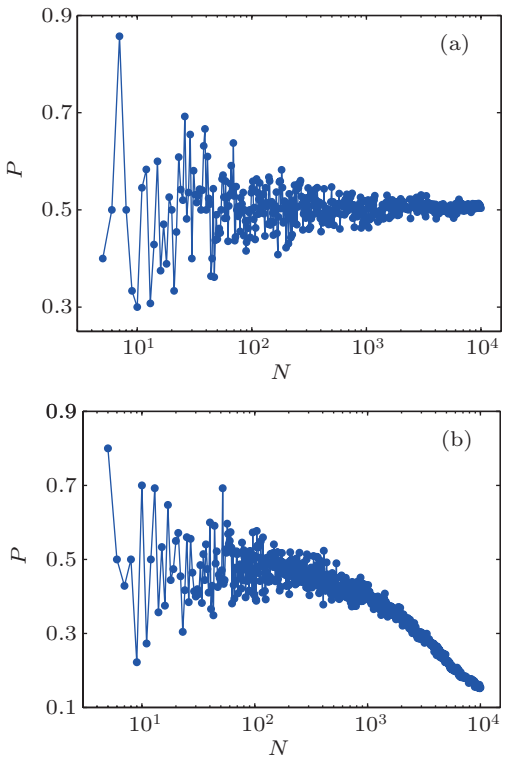


Fig. 4. (color online) Switching probability versus average times N. (a) Value of P converges to a probability value after N exceeds some critical value, indicating the proper choice of N. (b) Measurement result of an unstable system.

The readout pulse height is adjusted so as to maximize the difference of the switching probability between the two qubit states $|0\rangle$ and $|1\rangle$, the measurement fidelity. Due to the limited bandwidth of the SQUID current bias line, if the duration of the readout pulse is too short, the actual pulse height I_b that the readout SQUID receives will be much shorter than that at the input side. To determine the proper pulse duration time, we

measure the pulse height for 50% switching probability versus the pulse duration time (Fig. 5). We can see that the pulse height goes up rapidly as the pulse duration time becomes too short, this indicates the lower limit of the duration time of the readout pulse. The readout pulse in our measurements has a 1 ns rise time and a duration time of 10 ns, the hold plateau is 5 μs in duration.

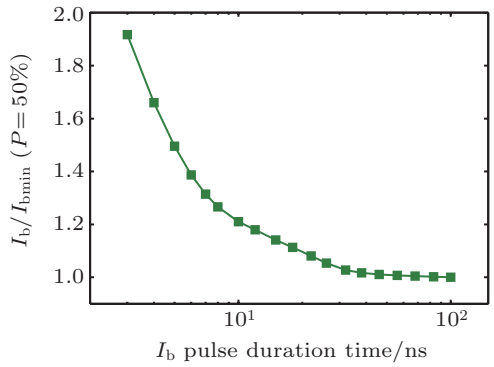


Fig. 5. (color online) Readout pulse height I_b for 50% switching probability versus pulse duration time.

Transitions between qubit states are induced by irradiating the qubit with microwave pulses. These microwave pulses are induced by an on-chip waveguide that is terminated at the end with an antenna. This microwave antenna is inductively coupled to the qubit loop. In spectroscopy and coherent state operation measurements, the microwave pulses are followed by the readout pulse to detect the final qubit state. These pulses are sent down to the sample through different cables, and this inevitably induces different time delays between them. So even if they are perfectly matched in time on the input side, they could be mismatched at the qubit side, and the difference can be as large as several tens of nanoseconds. Since the duration time of these pulses is on the order of nanoseconds, this difference is considerable in many cases. We make careful calibrations for these pulses to avoid the mismatch. Using the fact that under strong microwave irradiation, the critical current of the readout SQUID will be suppressed, resulting in a higher switching probability, for a very short readout pulse and a microwave pulse of some duration time, we measure switching probability P as a function of time delay between the ending of the microwave pulse and the start of the readout pulse t_{sp} and microwave power P_{mw} (Fig. 6(a)). The region where the switching probability increases with the microwave power is where the microwave pulse and the readout pulse overlap. Neglecting the very short readout pulse, we can clearly see that the delay time difference between these two pulses is about 18 ns. Adding this time difference when generating the pulses makes them perfectly matched at the qubit side. Since the microwave pulses should not induce suppression of the critical current of the readout SQUID, results of this measurement also indicate the proper microwave power to be used in the spectroscopy and coherent state manipulation measurement, that is, it should be somewhat below the microwave power in Fig. 6(a) where the switching probability starts to increase.

Calibrations for the time delay difference between the flux shift pulse and the readout pulse can be done in the same fashion. The microwave pulses not only need to be matched to the readout pulse in time domain, they must also have well defined pulse shapes at the qubit side. After going through several stages of attenuators and connectors, deformation of the microwave pulses might occur. To check for this, we measure switching probability P as a function of time delay between the end of the microwave pulse and the start of the readout pulse t_{sp} and microwave mixer control pulse amplitude V_{mx} at a microwave power that is strong enough to induce the increment of the readout SQUID switching probability. Figure 6(b) is the measurement result of using three equally separated microwave pulses; it shows the three microwave pulses at the qubit side with well defined pulse shapes as expected. This measurement result also indicates the proper microwave mixer control pulse amplitude V_{mx}.

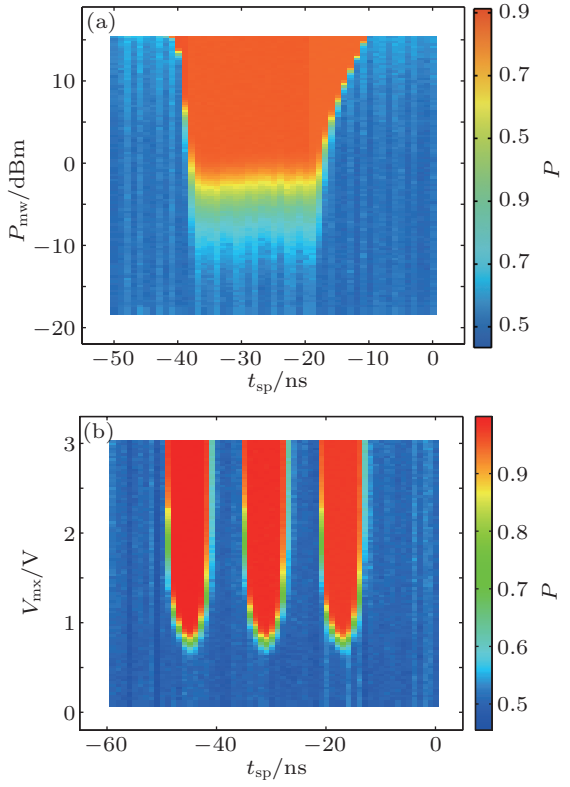


Fig. 6. (color online) (a) Switching probability P as a function of time delay between the ending of the microwave pulse and the start of the readout pulse t_{sp} and microwave power P_{mw}. The time delay difference between the readout pulse and the microwave pulse is −18 ns. (b) Switching probability P as a function of time delay between the ending of the microwave pulse and the start of the readout pulse t_{sp} and microwave mixer control pulse amplitude V_{mx}.

The first step in flux qubit measurement is to locate the qubit steps on the SQUID average switching current I_c versus applied magnetic flux Φ_e^* curve (Fig. 7(a)), where the

flux threading the qubit loop is $(n+1/2)\Phi_0$ (n is an integer). As the circulating current of the qubit changes sign at these points, they are revealed as tiny steps on the I_c–Φ_e^* curve (Fig. 7(a)). At the presence of microwave irradiation, the resonant absorption and excitation of the qubit from ground state $|0\rangle$ to excited state $|1\rangle$ will induce peaks/dips on the qubit steps (Fig. 7(b)). We use spectroscopy to map out the spectrum of the qubit. By applying 500 ns long microwave pulses of varying frequencies, we measure the switching probability of the readout SQUID at fixed pulse height for different magnetic flux biases Φ_e. If the qubit goes into resonance with the microwave, the qubit states $|0\rangle$ and $|1\rangle$ will be equally populated after the long microwave pulse irradiation, resulting in a switching probability change of the readout SQUID. Figure 8 is the measured spectrum of our single flux qubit. Due to the vanishing circulating current in the vicinity of $\Phi_0/2$, the spectrum line is not visible in this region, an adiabatic flux bias shift pulse has to be employed to measure the qubit response in this vicinity as mentioned before. The spectrum line can be well fitted with the hyperbolic formula $f = \sqrt{\Delta^2 + (2I_p(\Phi_e - \Phi_0/2)/h)^2}$. From the fitting, we can get $I_p = 160$ nA and $\Delta = 1.2$ GHz. Small kinks and breaks are visible on the spectrum line. This is due to the unstable magnetic environment of our measurement system, as the whole spectrum takes more than 24 h to acquire, drifts or sudden perturbations of the magnetic environment during this long period are reflected on the spectrum line.

We next perform coherent state manipulation measurement. By applying a resonant microwave pulse of fixed frequency and amplitude, Rabi oscillations[25] have been observed. The switching probability of the readout SQUID oscillates with the duration time of the resonant microwave pulse, indicating that the qubit state oscillates between $|0\rangle$ and $|1\rangle$. Figure 9 shows our Rabi oscillation measurement results in two different measurements. They are measured far away from the symmetric point of the spectrum, the so called optimal point where the qubit is most insensitive to flux noises. The data are well fitted with exponentially damped sinusoidal oscillations, with decay time $T_{Rabi} = 6$ ns for panel (a) and $T_{Rabi} = 78$ ns for panel (b). The main difference between these two measurements is the mutual inductance between the microwave antenna and the qubit loop M_{mq}, it is 125 pH in panel (a) and 0.05 pH in panel (b). The Rabi decay time is extremely short for panel (a) because M_{mq} in this measurement is too big, which leads to a strong coupling of the qubit to the external environment.

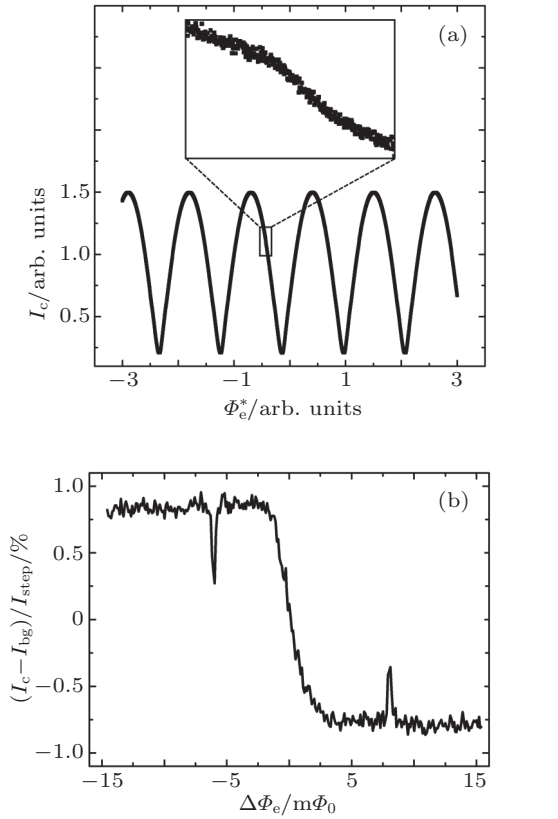


Fig. 7. (a) Readout SQUID average switching current I_c versus applied magnetic flux Φ_e^*. Inset shows an enlarged view of one qubit step. (b) Normalized qubit step at the presence of microwave irradiation. The microwave frequency is 7 GHz.

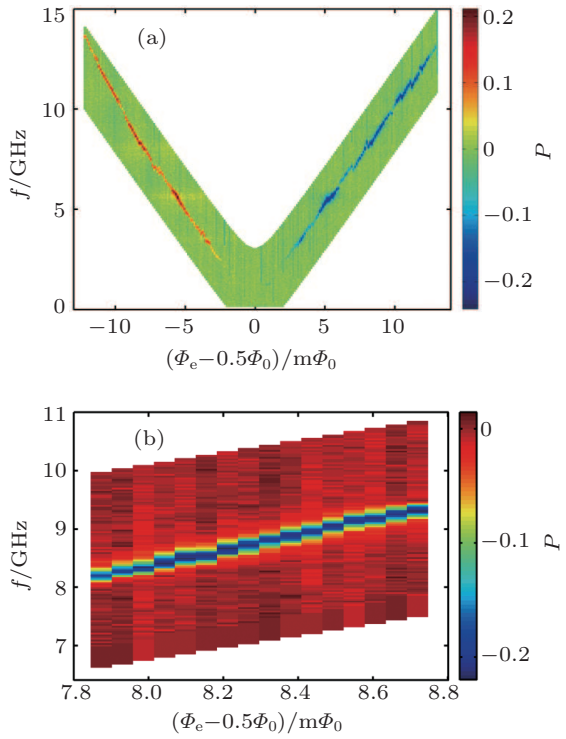


Fig. 8. (color online) (a) Energy spectrum of the single flux qubit sample. (b) Detail of the energy spectrum line (not measured at the same time with the energy spectrum in panel (a)).

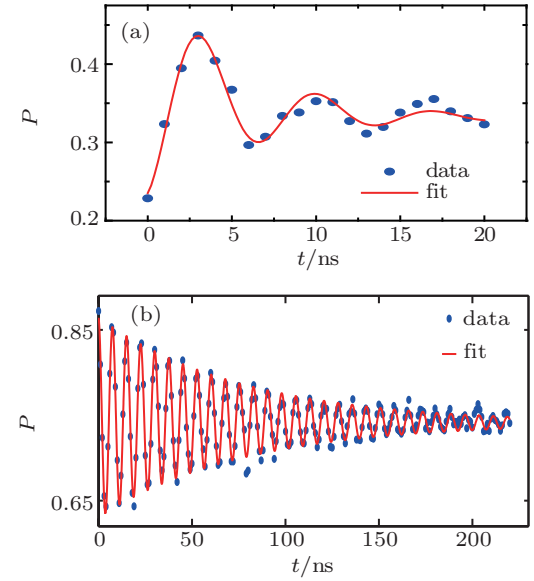


Fig. 9. (color online) Rabi oscillation measurement results in two different measurements; lines are exponentially damped sinusoidal fits to the data. The main difference between these two measurements is the mutual inductance between the microwave antenna and the qubit loop $M_{\rm mq}$, which is 125 pH in panel (a) and 0.05 pH in panel (b).

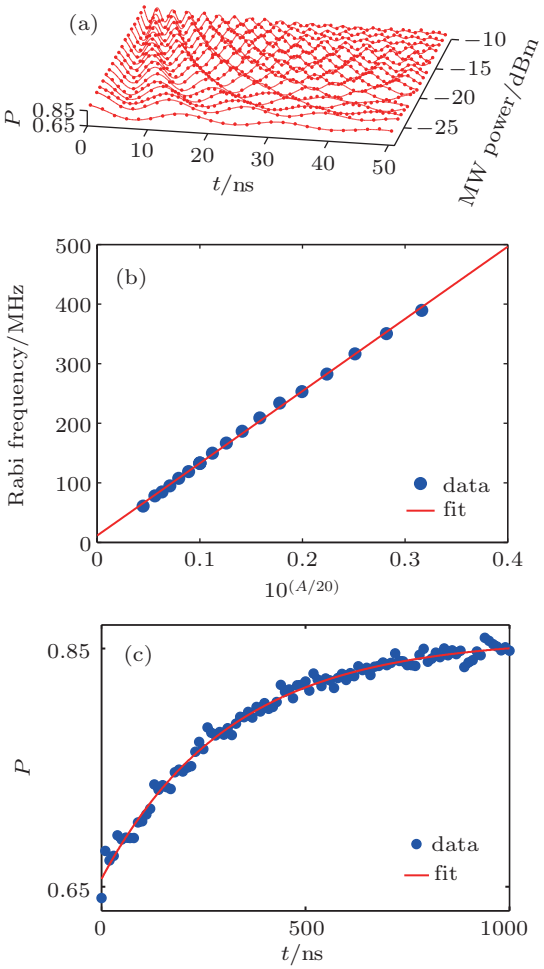


Fig. 10. (color online) (a) Rabi oscillations at different microwave powers; lines are exponentially damped sinusoidal fits to the data. (b) Rabi oscillation frequency vs. microwave amplitude; A is microwave power in arb. units; line is a linear fit. (c) Decay of the excited state; line is an exponential decay fit to the data with decay time $T_1 = 315$ ns.

By varying the microwave power, we measure the Rabi oscillations at different microwave powers (Fig. 10(a)). Figure 10(b) shows the Rabi oscillation frequency versus microwave amplitude. The key signature of the Rabi oscillation, a linear dependence of the oscillation frequency on the microwave amplitude, is clearly shown. We further study the relaxation of the qubit from the excited state. This is done by applying a coherent π pulse to rotate the qubit state from $|0\rangle$ to $|1\rangle$, waiting for some time, and performing the readout. Figure 10(c) shows the result, which shows an exponential decay of the $|1\rangle$ state occupation probability, with a relaxation time $T_1 = 315$ ns. The π pulse is determined by the Rabi oscillation measurement result above. The relaxation time is much longer than the Rabi decay time, indicating the extremely short dephasing time of our sample, as reflected in the fact that we do not observe any oscillation signals when we perform the Ramsey fringe measurement. We attribute the extremely short dephasing time to strong low frequency noises in our measurement system, as is also reflected on the kinks and breaks in the spectrum line.

To realize large scale quantum circuits, coupling between qubits is necessary. There are several ways to realize coupling between flux qubits, such as fixed inductive coupling, tunable coupling through a SQUID[26] or another flux qubit.[27] We present our spectroscopy measurement result on inductively coupled flux qubits. Figure 11(a) shows the coupled flux qubits sample. Three flux qubits are placed side by side in a shared edge arrangement to enlarge the mutual inductance for stronger coupling. The three flux qubits are designed to be identical, but the fabricated samples will always have slightly different parameters. We have performed spectroscopy measurements on this coupled flux qubits sample. Figure 11(b) shows the energy spectrum, two flux qubit spectrum lines are clearly visible on the spectrum. One branch of one of these spectrum lines has a deviation from the conventional hyperbolic shape, this might be the result of strong coupling between two of the three flux qubits. But as the spectroscopy signal is very weak and the spectrum line is not clear enough, we are not sure at this point.

In the measurement of this coupled flux qubits sample, besides the signal being very weak, the maximum switching current goes down as the magnetic coil current increases and the full width at half maximum (FWHM) of the switching distribution goes up as the magnetic coil current increases (Figs. 11(c) and 11(d)), indicating considerable heating of the magnetic coil current. So we have not carried out any further measurements like coherent manipulations of the qubit states.

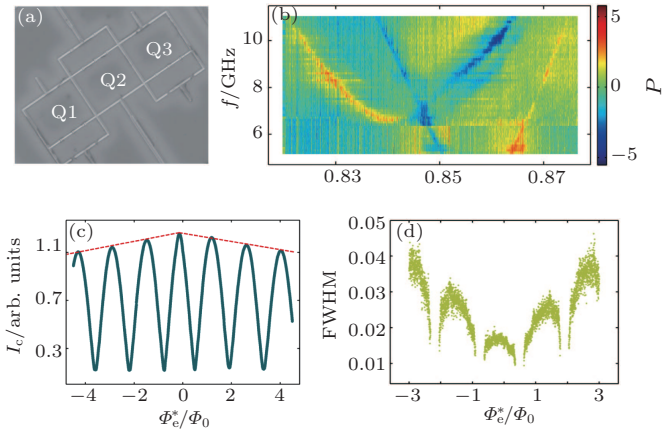


Fig. 11. (color online) (a) Scanning electron microscope (SEM) picture of the coupled flux qubits sample; the qubit loops are 15 μm×15 μm. (b) Energy spectrum of the coupled flux qubits sample. (c) The maximum switching current goes down as the magnetic coil current increases and (d) the FWHM of the switching distribution goes up as the magnetic coil current increases, indicating considerable heating of the magnetic coil current.

4. Conclusion

In conclusion, we have fabricated and performed quantum measurements on flux qubits. On single flux qubits, the measurement results show quantum energy levels and coherent Rabi oscillations, with Rabi oscillation decay time $T_{\text{Rabi}} = 78$ ns and $T_1 = 315$ ns. The coherence time determined from the Rabi oscillation depends strongly on the mutual inductance between the qubit and the microwave attenna. In practice, we should optimize the mutual inductance so that, on one hand, the electromagnetic interference from the microwave attenna would not reduce the coherence time substantially, on the other hand, the microwave power on the qubit is large enough for quantum manipulations. We have also performed spectroscopy measurements on inductively coupled flux qubits.

References

[1] Nielsen M A and Chuang I L 2000 *Quantum Computation and Quantum Information* (Cambridge: Cambridge University Press) pp. 2–12

[2] Gershenfeld N A and Chuang I L 1997 *Science* **275** 350

[3] Cirac J I and Zoller P 1995 *Phys. Rev. Lett.* **74** 4091

[4] Turchette Q A, Hood C J, Lange W, Mabuchi H and Kimble H J 1997 *Phys. Rev. Lett.* **75** 4710

[5] Makhlin Y and Schön G 2001 *Rev. Mod. Phys.* **73** 357

[6] Kane B 1998 *Nature* **393** 133

[7] Kane B E, McAlpine N S, Dzurak A S, Clark R G, Milburn G J, Sun He Bi and Wiseman H 2000 *Phys. Rev. B* **61** 2961

[8] Loss D and DiVincenzo D P 1998 *Phys. Rev.A* **57** 120

[9] Zanardi P and Rossi F 1998 *Phys. Rev. Lett.* **81** 4752

[10] Clarke J and Wilhelm F K 2008 *Nature* **453** 1031

[11] Josephson B D 1962 *Phys. Lett.* **1** 251

[12] Leggett A J and Garg A 1985 *Phys. Rev. Lett.* **54** 857

[13] Nakamura Y, Pashkin Y A and Tsai J S 1999 *Nature* **398** 786

[14] Vion D, Aassime A, Cottet A, Joyez P, Pothier H, Urbina C, Esteve D and Devoret M H 2002 *Science* **296** 886

[15] Mooij J E, Orlando T P, Levitov L S, Tian L, van der Wal C H and Lloyd S 1999 *Science* **285** 1036

[16] Orlando T P, Mooij J E, Tian L, van der Wal C H, Levitov L S, Lloyd S and Mazo J J 1999 *Phys. Rev. B* **60** 15398

[17] van der Wal C H, ter Haar A C J, Wilhelm F K, Schouten R N, Harmans C J P M, Orlando T P, Lloyd S and Mooij J E 2000 *Science* **290** 773

[18] Cong S H, Wang Y W, Sun G Z, Chen J, Yu Y and Wu P H 2011 *Chin. Phys. B* **20** 050316

[19] Jiang W, Yu Y and Wei L F 2011 *Chin. Phys. B* **20** 080307

[20] Hua T, Xu W W, Shi J X, An D Y, Sun G Z, Yu Y and Wu P H 2012 *Chin. Phys. B* **21** 098501

[21] Martinis J M, Nam S, Aumentado J and Urbina C 2002 *Phys. Rev. Lett.* **89** 117901

[22] Wu Y L, Deng H, Yu H F, Xue G M, Tian Ye, Li J, Chen Y F, Zhao S P and Zheng D N 2013 *Chin. Phys. B* **22** 060309

[23] Dolan G J 1977 *Appl. Phys. Lett.* **31** 337

[24] Tian Y, Yu H F, Deng H, Xue G M, Liu D T, Ren Y F, Chen G H, Zheng D N, Jing X N, Lu L, Zhao S P and Han S 2012 *Rev. Sci. Instrum.* **83** 033907

[25] Rabi I I 1937 *Phys. Rev.* **51** 652

[26] Plourde B L T, Zhang J, Whaley K B, Wilhelm F K, Robertson T L, Hime T, Linzen S, Reichardt P A, Wu C E and Clarke J 2004 *Phys. Rev. B* **70** 140501

[27] Niskanen A O, Nakamura Y and Tsai J S 2006 *Phys. Rev. B* **73** 094506